CHAPTER 12

MULTISPECTRAL IMAGING FROM MARS PATHFINDER

William H. Farrand, James F. Bell III, Jeffrey R. Johnson, Janice L. Bishop, Richard V. Morris

The Imager for Mars Pathfinder (IMP) was a mast-mounted instrument on the Mars Pathfinder lander which landed on Mars' Ares Vallis floodplain on July 4, 1997. During the 83 sols of Mars Pathfinders landed operations, the IMP collected over 16,600 images. Multispectral images were collected using twelve narrowband filters at wavelengths between 400 and 1000 nm in the visible and near infrared (VNIR) range. The IMP provided VNIR spectra of the materials surrounding the lander including rocks, bright soils, dark soils, and atmospheric observations. During the primary mission, only a single primary rock spectral class, "Gray Rock", was recognized; since then, "Black Rock", has been identified. The Black Rock spectra have a stronger absorption at longer wavelengths than do Gray Rock spectra. A number of coated rocks have also been described, the Red and Maroon Rock classes, and perhaps indurated soils in the form of the Pink Rock class. A number of different soil types were also recognized with the primary ones being Bright Red Drift, Dark Soil, Brown Soil, and Disturbed Soil. Examination of spectral parameter plots indicated two trends which were interpreted as representing alteration products formed in at least two different environmental epochs of the Ares Vallis area. Subsequent analysis of the data and comparison with terrestrial analogs have supported the interpretation that the rock coatings provide evidence of earlier martian environments. However, the presence of relatively uncoated examples of the Gray and Black rock classes indicate that relatively unweathered materials can persist on the martian surface.

12.1 Introduction

Between the success of the Viking landers in the late 1970's and the highly mobile Mars Exploration Rovers, Spirit and Opportunity, in the early 2000's, the Mars Pathfinder (MPF) mission provided high quality visible/near-infrared (400 – 1000 nm) multispectral observations from a stationary platform and *in situ* rock and soil major element chemistry measurements from the spacecraft's Sojourner rover. The landing platform hosted the Imager for Mars Pathfinder (IMP) stereo multispectral camera (Smith *et al.*, 1997) and the Sojourner rover was equipped with panchromatic wide-angle cameras and an Alpha Proton X-ray Spectrometer (APXS) (Rieder *et al.*, 1997; Foley et al,.2003, 2006).

The targeted landing site for the MPF lander was chosen to satisfy engineering and safety constraints, such as being below 0 km elevation and having an acceptably flat surface with moderate rock abundance. It was also selected on the basis of its scientific interest as a floodplain site in Chryse Planitia that received effluent from the Ares, Simud, and Tiu Vallis outflow channels (Golombek *et al.,* 1997a). These channels dissected Noachian-aged southern highlands and Hesperian-aged ridged plains and could

have brought materials from these units into the landing ellipse. The floodplain that encompasses the landing site itself was mapped as Hesperian in age (Tanaka *et al.*, 1997). Based on this geologic setting, a diversity of lithologies was expected at the landing site. Examination of Viking orbital color information prior to landing indicated that the landing site has a low red to violet ratio and an albedo intermediate between martian bright and dark regions. Based on these color characteristics, it was expected that rock surfaces would be largely dust-free and unweathered (Golombek *et al.*, 1997a). In post-landing studies, Wyatt *et al.*(2003) noted that the region is also intermediate between the basaltic "surface type 1" and, nominally, more andesitic and/or more weathered "surface type 2" spectral classes identified by the Mars Global Surveyor Thermal Emission Spectrometer (TES) (Bandfield *et al.*, 2000; Wyatt and McSween, 2002).

The spacecraft landed successfully on July 4, 1997 at approximately 19.13° N, 33.22° W. After landing, the MPF spacecraft was designated as the Sagan Memorial Station in honor of astronomer Carl Sagan. The spacecraft returned science data through 83 sols of surface operations. It achieved its mission objectives both in terms of length of surface operations, collection of multispectral imagery and *in situ* elemental analyses of rocks and soils by Sojourner's APXS instrument (Golombek *et al.*, 1997b). The landscape observed by the IMP at the MPF landing site largely agreed with pre-landing expectations of a rock-strewn landscape, with drifts of bright eolian dust, linear dunes with darker surfaces and scattered dark soils (Smith *et al.*, 1997b). In its general appearance, the landscape was very similar to floodplains observed at the mouths of terrestrial examples of catastrophic flood channels (Golombek *et al.*, 1999). While many of the rocks displayed surfaces coated with dust and/or indurated coatings, some rock faces and small cobbles appeared to be largely free of such coatings, allowing a more direct assessment of the primary rock mineralogy (*e.g.,* McSween *et al.*, 1999; Morris *et al.*, 2000; Murchie *et al.*, 2000; Farrand *et al.*, 2001; Bell *et al.*, 2002).

The IMP was designed to accomplish a large number of tasks. These included VNIR multispectral measurements of rocks and soils in the vicinity of the lander, the collection of monochrome, color, and stereo panoramas of the landing site, observations of the lander's magnet experiment, imaging of the Sun in order to measure atmospheric opacity, general atmospheric observations documenting the presence or absence of clouds, observations of the lander's wind socks for wind characterization, and stereo range finding and morphologic studies of rocks and surface deposits (Smith *et al.*, 1997a). The primary emphasis of this chapter is on IMP measurements of the multispectral reflectance properties of rocks and soils at the MPF landing site and on how the data have been used to provide key constraints on the mineralogy, origin, and evolution of the Ares Vallis region of Mars.

12.2 Imager for Mars Pathfinder instrument and data
12.2.1 Rationale for multispectral remote sensing on Mars Pathfinder
The IMP built on a heritage of visible and near infrared remote sensing of the surface of Mars. Telescopic observations of Mars had been made in the same visible to near infrared spectral range as well as at longer wavelengths (e.g., this volume, Calvin and Bell; Singer, 1985; Singer *et al.*, 1979). These observations had revealed the strong influence of ferric iron absorptions in martian bright region spectra causing a steep

absorption feature from the blue to red wavelengths with a relative reflectance maximum near 750 nm. This absorption edge was not as steep in the spectra of dark regions and observations extending out to 2 μm and beyond indicated the presence of ferrous iron absorption bands which could be attributed to mafic silicate minerals such as pyroxene and potentially olivine (Roush *et al.*, 1993). The Viking orbiters had provided three color information in the visible wavelengths (Klaasen *et al.*, 1977) and the Viking landers had provided multispectral visible and near infrared information (Huck *et al.*, 1977). The IMP built on this heritage. Its multispectral capability was used to provide information on spectral parameters such as red/blue ratios which provide information on the relative level of oxidation of surface materials (recalling the steeper blue-to-red slope of martian bright regions vis-à-vis those of the dark regions). Also, slope inflections in the blue to red region could also be used as a gauge of the relative level of oxidation of surface materials and this could be measured by the 530 nm band depth. The curvature of the spectrum in the 600 nm region could be indicative of the presence of other Fe^{3+} - bearing phases such as goethite which have a 660 nm absorption and this curvature can be assessed by the 600 nm band depth. Also, the presence of possible absorptions near 900 nm can be measured by calculation of the 900 nm band depth.

12.2.2 IMP instrument characteristics

The IMP consisted of a mast-mounted CCD focal plane array with optics separated by 15 cm for stereoscopic imaging capability. It utilized a 512 x 512 CCD that was split in half to accommodate measurements from each "eye". Identical 248 x 256 pixel subarrays were allocated to each eye resulting in a 14.4° x 14.0° field of view. The optics' angular resolution of 1 mrad/pixel yielded a spatial resolution of approximately 1 mm/pixel to 1 cm/pixel for objects 1 to 10 meters from the camera, respectively. Color information was provided in each eye by a filter wheel. Band centers and full width half maximum (FWHM) information for the resulting spectral channels are provided in Table 12.1. The 443 and 671 nm filters which are present in each eye, provided blue and red stereo coverage, respectively. These two filters plus 10 more at 480, 531, 600, 752, 802 858, 898, 931, 968, and 1003 nm constitute the 12 "geology bands" used for most multispectral assessments. Additional details about the IMP optics and electronics can be found in Smith *et al.*(1997a).

Table 12.1. Band centers and full width half maximum (FWHM) bandwidths of the IMP multispectral filters. All values are in nanometers.

Left Eye Filters		Right Eye Filters	
Center	FWHM	Center	FWHM
443	26	443	26
671	20	480	27
802	21	531	30
858	34	600	21
898	41	671	20
931	27	752	19
968	31	967	30
1003	29		

12.2.3 Data processing and calibration

The IMP was calibrated before launch with extensive characterization of its electronic and optical characteristics. IMP data were calibrated based on preflight calibration coefficients and measurements made during surface operations of on-board calibration targets (Reid *et al.*, 1999). The estimated radiometric accuracy of IMP data was > 95% over all wavelengths (Reid et al, 1999). Calibration of the radiometric response of the IMP during surface operations was conducted using a calibration target consisting of three concentric rings of white, gray and black (reflectance of approximately 0.05, 0.4 and 0.95), which were produced by embedding rutile and carbon black in varying percentages in a silicone matrix. Color targets were also provided to assess the IMP's spectral response. These consisted of chips with hematite (red), maghemite (brown), goethite (yellow), chrome dioxide (green), and cobalt (blue) pigments embedded in silicone. Surface measurements of the reflectance of the color chips provided excellent agreement with surface measurements of their reflectance spectra (Reid *et al.*, 1999).

Calibration during surface operations consisted of correction for instrumental sources of noise followed by comparison of the measured response from the gray level rings of the calibration target to the measured laboratory reflectance of the rings (Reid *et al.*, 1999). Measurements of calibration target images acquired close in time to scene acquisition were used to convert the data at each band pass to apparent radiance factor. Radiance factor is defined by (Hapke, 1993, p. 262) as the ratio of the bidirectional reflectance of a surface to that of a perfectly diffuse surface illuminated at 0 degree incidence angle. As noted by Reid *et al.*(1999), the calculated radiance factor values did not strictly meet the Hapke (1993) definition of that quantity since the diffuse sky illumination was included in the calibration in addition to the direct solar illumination. Most of the work presented here utilized the quantity "relative reflectance" or R*, which is the radiance factor divided by the cosine of the solar incidence angle (Reid *et al.*, 1999; Bell *et al.*, 2000). This is equivalent to the Hapke (1993) quantity of "reflectance factor", which is defined as the ratio of the reflectance of a surface to that of a perfectly diffuse surface under the same conditions of illumination and emittance angle. However, because different rock and soil surfaces in any measured scene are likely to deviate from the illumination and emission geometry of the calibration target the values do not meet the strict Hapke (1993) definition of reflectance factor, thus the use of the term "relative reflectance".

12.2.4 Data collection

Over the course of the MPF mission, 16,661 images were returned from the IMP (Golombek *et al.*, 1999). The types of data products are discussed next.

12.2.4.1 Panoramas

Five panoramas of landscape around the lander (Table 12.2) containing over 3,500 component image frames, were collected over the course of the MPF mission (Gaddis *et al.*, 1999). On the first sol of the mission, before extension of the IMP's mast or deployment of the Sojourner rover, a partial "Mission Success" panorama in 3 right eye bands and one left eye band (for red stereo) was collected and transmitted to Earth

with lossy compression. A losslessly compressed "Insurance" panorama was also acquired prior to mast deployment. The panorma was obtained with 3 right eye bands plus stereo coverage in blue filters (Herkenhoff *et al.*, 2003). After mast deployment, the IMP acquired other panoramas with some gaps in spatial and spectral coverage, including the 3-color "Monster Pan" and "Gallery Pan" and the "Super Pan", which is a nearly comprehensive 360° view around the lander in all 12 geology filters, transmitted at an approximately 2:1 compression ratio (Gaddis *et al.*, 1999). The Super Pan is composed of eight component octants, labeled S0181 – S0188. Each octant is, in turn, composed of component segments. Because of the relatively small size of the IMP focal plane array, limited spacecraft memory and limited downlink capacity, these component segments were collected piecemeal starting on sol 13 of the mission, with image acquisitions continuing until communication was lost with the spacecraft. The Super Pan was 83% complete at the time that communication was lost. Because of the long time of acquisition of the Super Pan, adjacent component segments were often collected under different solar and sky illumination conditions. Small amounts of airfall-deposited dust also accumulated on the IMP calibration target over the course of Super Pan acquisition, slightly affecting the resulting calibration to R* (e.g., Johnson *et al.*, 2003). A final version 3 calibration of the Super Pan image cube was carried out by Murchie *et al.*(2003) which included correction of registration errors and correlation of relative calibration for neighboring frames to the S0184 illumination conditions.

Table 12.2. IMP Panoramas

Pan Name	Azimuthal coverage	Elevation coverage (# of tiers)	Bands used	Compression
Mission Success	180° red stereo; 180° color	1	Right: 5R, 9R, 0R (670, 530, 440 nm) Left: 670 nm	Lossy
Insurance	360°	3	Right: 750, 600, 530, 440 nm Left: 440 nm	Lossless
Monster	360°	4	Right: 670 nm (all tiers), 930, 440 nm (middle two tiers) Left: 670 nm	Lossy
Gallery	360°	3	Right: 930, 670, 440 nm	Lossy
Super	360°	4	All geology filters	Lossless of Red and Blue stereo; Lossy (2:1) of remaining bands

12.2.4.2 Multispectral spot collection

Over the course of the mission, 58 small spatial areas were imaged in all 12 geology filters in small 64 pixel x 64 pixel "multispectral spot" (MSS) observations. A full list of these observations is provided in Table 12.3 of Bell *et al.*(2000). The materials imaged in these MSS observations were characterized in terms of their overall 12 point

spectra and in terms of spectral parameters derived from those spectra (Table 12.3). For convenience, we refer to the relative reflectance at a given wavelength as, for example, "R_{670}", for the R* value at 670 nm. To be consistent, we adopt this terminology in this review. More advanced processing techniques applied to the IMP multispectral data in more recent, post-mission, studies are summarized below.

Table 12.3. Relevant Spectral Parameters used in the characterization of IMP data that are referenced in this paper.

Spectral Parameter	Definition
Red/Blue ratio	R_{670} / R_{440}
530 nm Band Depth	$1 - [R_{530} / (0.609 \times R_{440} + 0.391 \times R_{670})]$
600 nm Band Depth	$1 - [R_{600} / (0.5 \times R^*_{530} + 0.5 \times R_{670})]$
900 nm Band Depth	$1 - [R_{900} / (0.5 \times R_{800} + 0.5 \times R_{1000})]$

12.2.4.3 Other IMP observations

Other observations made by the IMP included atmospheric measurements (Smith and Lemmon, 1999 and references contained therein), wind sock observations (Sullivan *et al.*, 2000), astronomical observations (Thomas *et al.*, 1999; Murchie *et al.*, 1999), surface photometry observations (Johnson *et al.*, 1999), and observations of MPF's magnetic properties experiment (Madsen *et al.*, 1999).

12.3 IMP results
12.3.1 General results

As was noted above, the geologic setting observed by the IMP at the MPF landing site consisted of a rock-strewn landscape, with drifts of bright eolian dust, small linear eolian bedforms with darker surfaces and scattered dark soils (Golombek *et al.*, 1999a). Rocks observed by IMP exhibited red/blue color ratios consistent with varying degrees of dust coatings. Northeastern facing rock surfaces often exhibited the lowest red/blue ratios and were thought to be the most dust-free because these rock surfaces face into the prevailing wind direction (McSween *et al.*, 1999). Downwind rock faces typically appeared dustier. The types of rock coatings observed by the IMP have since been used to draw inferences about past environments in the vicinity of the landing site (McSween *et al.*, 1999; Barnouin-Jha *et al.*, 2000; Bishop *et al.*, 2002).

12.3.2 Rocks
12.3.2.1 Gray Rock

Initial studies of rocks present at the MPF landing site (Smith *et al.*, 1997b, McSween *et al.*, 1999) described several spectral classes of rocks, some of which actually referred to rock coatings. Despite pre-landing expectations that there might be an assemblage of different lithologies present at the landing site, the initial interpretation was that there was only a single spectral class that encompassed all those rock surfaces which were the least dusty. This was known as the "Gray Rock" spectral class. Brighter, presumably dustier coatings on downwind rock surfaces were characterized as "Red" and "Maroon" rock spectral classes. In addition, a "Pink" rock class was recognized which was characterized as either another form of coating or, quite possibly, an indurated soil (the Sojourner rover scuffed the surface of a Pink Rock and the results indicated that

it was likely an indurated soil). In terms of Gray Rock's spectral properties, it was characterized by a low red/blue ratio and low 530 nm band depth. Both of these characteristics were interpreted as indicating the presence of predominantly ferrous iron mineral phases, based on previous multispectral image studies and laboratory analog investigations (*e.g.,* Arvidson *et al.*, 1989; Bell *et al.*, 2000; Morris *et al.*, 2000). The peak reflectance in Gray Rock spectra is at 750 nm with a flat to negative sloping continuum at longer wavelengths. These spectral characteristics were interpreted as indicating either the lack of a mineral phase with an absorption in the 900 to 1000 nm range or the presence of a mineral phase whose band minimum occurs at, or longwards, of the longest IMP band centered at 1003 nm. Named rocks representative of the Gray Rock spectral class were "Booboo", "Stimpy", and "Shark". Representative Gray Rock spectra are shown in Figure 12.1.

Morris *et al.*(2000) compared Gray Rock spectra to terrestrial analog materials and noted three possible explanations for the negative NIR slope and lack of a well defined long wavelength absorption in Gray Rock spectra. First, the rocks could contain high-Ca pyroxene and/or olivine, both of which have band minima at or beyond the IMP camera's sensitivity range near 1000 nm. Second, the rock surfaces could contain mechanical mixtures of nanophase ferric oxides in combination with a reflectance-lowering opaque phase such as magnetite (Morris and Neely, 1982). The third possibility was that the negative slope could be caused by a thin ferric oxide coating on a dark substrate (*e.g.,* Fischer and Pieters, 1993; Johnson and Grundy, 2001). Murchie *et al.*(2003) suggested that Gray Rock might be a weathered basalt containing a significant fraction of phyllosilicate minerals in its surficial weathering rind. This interpretation would mirror the interpretation by Wyatt *et al.*(2002) of the so-called "surface type 2" lithology first identified by Bandfield *et al.*(2000) using data from the Thermal Emission Spectrometer aboard Mars Global Surveyor. While Bandfield *et al.*(2000) had interpreted the surface type 2 spectrum as being caused by an andesitic lithology, Wyatt *et al.*(2002) suggested that the spectrum is also consistent with a phyllosilicate-rich weathering rind on a more mafic basalt (although others have suggested alternative explanations; *e.g,* Hamilton *et al.*, 2003). Phyllosilicates lack diagnostic spectral features in the wavelength range covered by IMP, thus they, possibly with accompanying opaque minerals, could act to mask a pyroxene band as was suggested by Murchie *et al.*(2003).

It has also been suggested from thermal infrared studies (Kraft *et al.*, 2003) that Gray Rocks' relatively high SiO_2 abundances may result from a coating of opaline silica. Such a silica coating could also mask a pyroxene absorption feature. Some dark-colored basaltic Hawaiian lava rocks with thin and shiny silica coatings exhibit reflectance maxima near 600-700 nm and negative NIR slopes; however, light-toned ceramic-like silica coated Hawaiian rocks have a relative reflectance maximum at a shorter wavelength (near 600 nm; Bishop *et al.*2003; Minitti *et al.*2003; Deal *et al.*2003), which is shorter than that observed in spectra of Gray Rocks.

Representative terrestrial analog spectra of several types of materials posited as being analogous to the Gray Rock surface are plotted in Figure 12.2. These include the clinopyroxenite SNC meteorite Nakhla (Morris *et al.*, 2000), a silica coating (Bishop *et al.*, 2003), and the <1 mm size fraction of palagonitic tephra HWHP301 (Morris *et al.*, 2000). All of these materials have a negative slope in the NIR without a well defined

band minimum in the IMP wavelength range, but none, by themselves, represent an ideal match to the Gray Rock spectrum.

12.3.2.2 Black Rock

Murchie *et al.*(2000) recognized several near-field examples of an additional rock spectral class that they named "Black Rock" and a single example of another rock spectral class referred to as "Orange Rock". Black Rock and Orange Rock spectra are shown in Figure 12,3. The Black Rock spectral class differs from the Gray Rock spectral class in that it has a relative reflectance maximum near 670 nm, versus Gray Rock's 750 nm reflectance peak, and a relatively strong long wavelength absorption band centered near 930 nm where the Gray Rock had a weak absorption at or longwards of 1000 nm. Black Rock examples also have a very low red/blue ratio (< 3.5). The Orange Rock spectrum has a 750 nm relative reflectance maximum and a long wavelength absorption band center near 900 nm. Murchie *et al.*(2000) posited that the Black Rock examples might contain more orthopyroxene or a combination of low-Ca clinopyroxene (possibly with olivine), or a ferric mineral in combination with a low albedo lithology. Out of a set of SNC meteorite spectra, Wright *et al.*(2005) found the NIR Black Rock spectra to match well with that of Dar al Gani (DaG) 735 meteorite. The DaG shergottites are mostly composed of pigeonite with a significant fraction (14-20%) of Mg-rich olivine megacrysts (Zipfel *et al.*, 2000, Wadwha *et al.*, 2001). In contrast, the spectrum of Orange Rocks are more consistent with a dust layer coating the rocks as there is a maximum near 750 nm and minimum near 920 nm typical of many of the alteration materials suggested as constituents of coatings (*eg*., McSween *et al.*, 1999; Barnouin-Jha *et al.*, 2000).

Spectrally distinct Black Rock spectral sub-classes were noted by Bell *et al.*(2002) and were detected through application of a spectral mixture analysis methodology (*e.g.*, Adams *et al.*, 1986, 1993; Bell *et al.*, 2002; Farrand *et al.*, 2006). Spectral mixture analysis (SMA) is an approach that models the measured signal from each spatial element as a linear combination of component "endmember" spectra. Only a small number of endmembers are needed to model each pixel spectrum and, by definition, the number of endmembers can be no more than one more than the number of image bands available. The relevant equation of SMA, in vector format is:

$$R = a\mathbf{B} + e$$

Where R = the measured spectrum from the spatial element or pixel, in the Bell *et al.*(2002) study, the values for each pixel were in R*; a = a vector of fractions, one for each endmember used in the model; $\mathbf{B}$ = a matrix of endmember spectra; e = the vector of offset or residual values between the modeled, best fit, spectrum and the measured pixel spectrum. The end result of SMA is a series of "fraction" images, one for each endmember, and a root mean square (RMS) error image that encapsulates the error of the fit. The fraction images have digital numbers (DN) ideally between 0 and 1 where pixels with a DN of 0 are devoid of the endmember material and pixels with a DN of 1 are filled with the endmember material. In the form of SMA applied in the Bell *et al.*(2002) study, the endmembers used were "image endmembers" these are single pixel spectra or, more commonly, averages of a small number of pixel spectra that were taken to represent the best examples of each of the spectral endmembers. In the analysis of the Super Pan data, left and right eye data were analyzed separately and each image segment making up the Super Pan was analyzed individually. For both left and right eye data, there were

generally three endmembers used: shade, bright dust, and rock. Shade is a non-material endmember that encompasses the effects of topographic shadowing and, to some extent, diffuse illumination since shade pixels are extracted from the least illuminated, shadowed areas available in each scene. The residuals from each band can be captured in a single root mean square (RMS) error image which represents the goodness of fit of the modeled endmember to the data. Materials with spectra very different from those of the endmember spectra will have high RMS error values. Representative fraction images and an example of a RMS error image detection of a Black Rock occurrence are shown in Figure 12.4.

Larger (boulder-sized) occurences of Black Rock in the far field of the Super Pan were noted by Murchie *et al.*(2003) and described in more detail by Farrand *et al.*(2004). Figure 12.5 shows examples of Black Rock boulders mapped by Farrand *et al.*(2004) through the application of a constrained energy minimization (Farrand and Harsanyi, 1997) methodology. The constrained energy minimization (CEM) approach is related to the SMA approach in that it determines the fractional abundance of some endmember or target material. However, unlike SMA, not all endmember materials need be identified. Instead the scene is essentially decomposed in terms of a desired target spectrum and undesired background spectra. Pixels devoid of the target signature are constrained to be nulled to zero and those pixels that are identical to the target signature are constrained to equal one. Application of the CEM methodology in this instance was very useful since the Black Rock occurences represent an areally minor portion of the image scene and thus could not be well modeled as endmembers; i.e., as materials that significantly contributed to the signal from pixels across the scene.

12.3.3 Soils

McSween *et al.*(1999) briefly discussed soils at the MPF landing site. Soils mentioned by these authors included "Bright Red Drift", which was characterized by a steep blue to red slope, a reflectance maximum at 750 nm and a lack of a near infrared absorption feature. The other soil class mentioned by these authors was "Brown Soil" which has a lower albedo, a reflectance peak at 800 nm and a weak near infrared absorption band. In the first comprehensive discussion of soil spectral properties at the MPF landing site, Bell *et al.*(2000) subdivided soils at the site into eight spectral classes. These classes were determined on the basis of partitioning clusters observed in 2-dimensional histograms of parameters derived from multispectral spot observations. Spectra of these classes are shown in Figure 12.6. These classes include four different Bright Soil classes, Surface Dust, Atmospheric Dust, Dark Soil, and Disturbed Soil.

The class with the widest spatial distribution, and most closely linked to the McSween *et al.*(1999) "Bright Red Drift" is the "Bright I" class. It is characterized by a high red reflectance, a high red/blue ratio, and a flat to slightly negative NIR slope. Bright I soil spectra were interpreted as poorly-crystalline Fe-rich dust and only minor amounts of mafic minerals. The "Bright II" class is somewhat less abundant, and is generally similar to the Bright I class except that it has a generally stronger long wavelength absorption between 800 and 1000 nm. The stronger NIR band in these soils was interpreted as indicating a greater abundance of crystalline ferric or ferrous minerals compared to Bright I soils. The "Bright III" and "Bright IV" classes are less abundant but are spectrally similar in that they have convex spectral shapes in the NIR with a

relative reflectance maximum near 754 nm for the Bright III soils and near 800 nm for the Bright IV soils. Both Bright III and Bright IV soils were interpreted to consist of significant mafic minerals, perhaps mixed (Bright III) or coated (Bright IV) by Fe-rich dust or weathered coatings. The "Surface Dust" unit is also rare and is characterized by a positive slope from 800 to 1000 nm. This material was interpreted as almost "pure" nanophase ferric oxide dust, with no discernable mafic signature. The "Atmospheric Dust" unit is from a measurement of the sky, and exhibits a high blue reflectance and a low red/blue ratio, similar to the skylight spectrum described by Thomas *et al.*(1999). Like Surface Dust, Atmospheric Dust was not found to exhibit any discernable mafic spectral signature in IMP data.

The darker soil units described by Bell *et al.*(2000) were interpreted as being coarser-grained, compacted, and/or mixed with a larger amount of dark ferrous materials relative to bright materials. The set of dark soil units included "Dark Soil", and "Disturbed Soil". "Dark Soil" has a low reflectance in the red and NIR, a high reflectance in the blue (relative to the bright soil units described above), and a negative slope from 800 to 1000 nm. A near infrared absorption feature is weak or absent. This material has been interpreted as being spectrally dominated at IMP wavelengths by coarser-grained ferric-rich material and perhaps a minor mafic component. The "Disturbed Soil" unit, exposed in places by the action of the rover wheels or lander airbags, is also low in its red and NIR reflectance but has a lower reflectance in the blue than does the "Dark Soil" unit. It also has a weak NIR absorption band. These characteristics lead to the interpretation of Disturbed Soil spectra as consistent with the presence of coarser-grained and/or more crystalline ferric or ferrous minerals compared to "normal" Bright I Soils and Dark Soils. The Disturbed Soil spectrum of Bell *et al.*(2000) is essentially the same as the Brown Soil noted by McSween *et al.*(1999) although occurences of Brown Soil include locations not disturbed by the lander airbags or rover activity.

Among the soils containing a discernable long wavelength absorption are dark soils coating linear dunes such as "Mermaid" dune. Morris *et al.*(2000) noted the similarity of the 930 band observed in spectra of Mermaid Dune and related materials to that observed for the Oxia Palus region (Mustard *et al.*, 1997) and for orthopyroxene- and pigeonite-bearing SNC meteorite samples (Figure 12.7). This association suggested to Morris *et al.*(2000) that these soils might be spectrally dominated by low-Ca pyroxenes. Results from the Mars Express OMEGA (Observatoire pour la Minéralogie l'Eau les Glaces et l'Activité) imaging spectrometer have indicated higher fractions of low-Ca pyroxenes in the southern highlands of Mars (see Bibring *et al.*, this volume; Mustard *et al.*, 2005). Thus, it is possible that the materials coating Mermaid dune and similar features might be derived from rocks similar to those found in the southern highlands. The Sojourner rover lacked a microscopic imager to determine the grain size of the surface coating of dunes such as Mermaid; however, Moore *et al.*(1999) suggested that the soils in Mermaid were poorly sorted mixtures that contained granules down to fine-grained dust. By association with dunes examined by the Spirit rover (*e.g.,* Greeley *et al.*, 2004; Farrand *et al.*, 2005) suggested that the Mermaid dune type of coating might similarly consist of an armoring of small basalt pebbles.

In spectral mixture analysis of component Super Pan scenes, Bell *et al.*(2002) noted that aprons of high relative fractional abundances of rock occurred in the soil

around some rocks. These aprons were dubbed "Rock Soil" and were interpreted as the consequence of mechanical weathering of the rocks and the subsequent accumulation of small rock fragments in the soil nearby. This observation is consistent with an observation by Morris *et al.*(2000) that all the observed MPF soils have some contamination by ferrous oxide-rich rock fragments and, likewise, that observed rocks were all contaminated by some ferric oxide-rich dust. These authors noted that MPF soils had R_{750}/R_{445} values > 4.0 (average value of 5.7 ± 1.2) and rocks had R_{750}/R_{445} values < 4.0 (average value of 2.9 ± 0.6). This red/blue ratio evidence is consistent with a highly oxidized, ferric iron rich nature for the MPF soils and a more ferrous iron-rich nature for the MPF rocks. The contamination of rock surfaces by ferric oxide rich dusts was illustrated by comparison to SNC meteorite samples, which do not display a significant ferric absorption edge and have a low R_{750}/R_{445} value of 1.3 ± 0.2 (Morris *et al.*, 2000).

Various terrestrial analogs and components have been proposed to account for the observed reflectance properties of soils observed by IMP. In Figure 12.8a, Bright Drift soil spectra from the S0182 and S0185 octants are compared with a soil from the summit of Haleakala volcano in Maui (Hal-399, Bishop *et al.*, 2006) and the less than 1 mm fraction of the JSC-1 Mars analog spectrum (Allen *et al.*, 1998; Morris *et al.*, 2000). The spectrum of the altered Haleakala fines is about as bright as the martian bright soils, but has less spectral character and similar behavior is observed in the JSC-1 spectrum. The Hal-399 sample is primarily composed of amorphous and poorly crystalline alteration products of volcanic glass and basaltic lava. Likewise, the JSC-1 sample is composed of ash particles with the majority of iron present as nanophase ferric oxides (Morris *et al.*, 2000). While the terrestrial analogs for the Bright Drift are fairly good matches, the nature of the Brown Soil material has more uncertainty. A number of materials with 930 nm band minima, and band widths, that resemble that in Brown Soil are shown in Figure 12.8b. These include a jarositic tephra from Mauna Kea (HWMK 515; Morris *et al.*, 2000), a maghemite sample (MHS-3; Morris *et al.*, 2000) and a ferrihydrite (Bishop *et al.*, 1998). The Brown Soil has been observed to have some spectral character in common with the "Maroon Rock" spectral class and the latter class and other rock coatings is discussed next.

12.3.4 Rock coatings

In addition to the Gray Rock spectral class, early studies of the IMP data noted additional classes of "Red Rock", "Maroon Rock", and "Pink Rock" (*e.g.*, Smith *et al.*, 1997b; McSween *et al.*, 1999). The first two classes occur on rocks with "clean" Gray Rock faces and, thus, the "red" characteristics of these classes were interpreted as coatings (McSween *et al.*, 1999). Pink Rock was interpreted as either hardpan, encrusted drift materials, or indurated soil (McSween *et al.*1999; Moore *et al.*, 1999). Spectra of Maroon, Red, and Pink Rock examples are shown in Figure 12.9.

Red Rock surfaces have higher relative reflectance, higher red/blue ratios, and a stronger 530 nm band depth than Gray Rocks. Red Rocks have higher reflectances at short wavelengths than bright drifts and bright soils, but comparable reflectances and spectral properties in the NIR. Named rocks which have some surfaces with spectra representative of the Red Rock spectral class are "Half Dome", "Broken Wall", and "Wallace". Like the Red Rock faces, Maroon Rocks have high red/blue ratios and strong

535 nm band depths, but are lower in albedo than Red Rocks. Unlike Red Rocks and Gray Rocks, however, Maroon Rocks have a reflectance maximum at 800 nm and a weak absorption band at 900 to 930 nm. Named rocks representative of the Maroon Rock spectral class included the downwind side of "Yogi", "Flipper", and "Valentine." The type specimen for Pink Rock is the rock "Scooby Doo" which lies northeast of the MPF lander. While generally similar in spectral shape to bright drifts and soils, Pink Rocks are higher in reflectance in all IMP bands. Pink Rocks can also be distinguished from bright drifts and soils by their higher reflectances at the shortest wavelengths.

Spectral parameter plots by McSween *et al.*(1999) revealed a primary and a secondary spectral trend between MPF rock classes. In Figure 12.10, 900 nm band depth vs. red/blue ratios show a primary trend of low red/blue ratio and high 900 nm band depth for Gray Rocks and Red Rock faces. A secondary trend, exhibiting a high red/blue ratio and low 900 nm band depth, was found for Pink Rocks, Maroon Rocks and Brown Soils. The majority of rocks observed at the landing site follow the primary trend (McSween *et al.*, 1999). McSween *et al.*(1999) show additional spectral trends and inter-relationships among rock classes in their plots of 900 nm band depth vs. 530 nm band depth and of red/blue ratio vs. 670 nm reflectance. The "primary trend" was interpreted as resulting from coatings of eolian dust on Gray Rock surfaces. The spectral behavior of the "secondary trend" materials has been interpreted by McSween *et al.*(1999) as resulting from the presence of a mineral phase not seen in the "primary trend" materials-possibly a ferrihydrite, maghemite, or composite of ferric and ferrous phases such as those observed in impact melt rocks from Manicouagan Crater (Morris *et al.*, 1995).

A three stage model was proposed by McSween *et al.*(1999) to explain the spectral classes of rocks and soils observed at the MPF landing site. In the first stage, an initial Brown Soil layer was overlain by large rocks which had, or in this stage developed, "Maroon" coatings. These rocks may have been from local volcanic sources, or may have been transported to the site during one of the catastrophic Ares Vallis flood events (*e.g.,* Golombek *et al.*, 1997; Tanaka, 1997). In stage two, smaller, largely uncoated rocks and cobbles were emplaced, possibly as a result of impact events or mechanical weathering of larger, older rocks. During this stage, bright red drifts formed a relatively uniform surficial soil layer at the site. In stage three, the action of wind redistributed some of the red drift material into dunes and some of it coated rocks to form the Red Rock and possibly Pink Rocks classes. The wind action also partially removed the Maroon coatings, formed during the first stage, from the large rocks. This model accounts for the primary and secondary spectral trend differences of Red Rocks and Maroon Rocks by positing that the two different types of coatings, with different mineral constituents, were emplaced in different periods of time and, potentially, in different paleoenvironments.

The correlation of the spectral properties of coated rocks with APXS-determined chemistry was examined by Bridges *et al.*(2001), who found a roughly linear trend of red/blue ratio vs. SO_3 for MPF rocks and soils. The reddest rock surface examined, A-7 on Yogi, had the most sulfur and the bluest rock surface examined, A-17 (Shark) had the least sulfur. Because the sulfur content is assumed to be low in primary igneous rocks on Mars (*e.g.,* McSween *et al.*, 1999), this correlation was interpreted as being consistent with essentially all of the rock surfaces having varying degrees of "contamination" by ferric- and sulfur-bearing dust coverings and/or coatings. Barnouin-Jha and Murchie

(2000) and Bridges *et al.*(2001) also noted that the rock surfaces facing toward the northeast, the direction from which the strongest winds originate, have lower red/blue ratios and, among those examined with the APXS, are lower in sulfur. These northeast-facing rocks were interpreted to have relatively thinner dusty/ferric coatings compared to other rocks. Observations by the Mars Exploration Rover Spirit's APXS and Mössbauer spectrometers have shown that bright drift deposits at Spirit's Gusev crater landing site have the most sulfur and Fe^{3+} of basaltic surface materials (Morris *et al.*, 2006); thus the model of drift-coated rocks at the MPF site being more S-rich is a consistent observation.

Barnouin-Jha *et al.*(2000) noted that since the 530 nm band depth is lower for coated rocks than it is for bright drift with a comparable red/blue ratio, then hematite might be more prevalent in the drifts and goethite might be more prevalent in the coated rocks with the strong 600 nm shoulder. Similarly, Murchie *et al.*(2001) interpreted the Maroon Rock coatings with the stronger 600 nm inflection as being bright red drift cemented to the rock surfaces with an additional ferric oxide phase, suggested to be goethite. However, neither the IMP nor other instruments on the MPF mission were able to provide definitive identification of specific ferric iron mineral phases.

Ward *et al.*(1999) and Murchie *et al.*(2001) categorized rocks at the landing site into shape classes (knobby, lobate, angular, equant, and tabular) and size classes (pebbles, cobbles, boulders). The knobby rocks were defined as rocks with rounded to angular protuberances and/or sockets. Lobate rocks were similar to the knobby rocks but with larger protuberances. Angular rocks had well defined angular edges. Equant rocks were rounded to subangular. Tabular rocks were those with a high aspect ratio and a planar surface. Flat rocks were similar, but nearly buried. Pebbles were defined as those less than 6 cm in diameter and boulders were larger than surrounding rocks and sometimes elongated in shape. Murchie *et al.*(2001) noted that tabular, angular, and equant rocks displayed a stronger 600 nm inflection than lobate and knobby rocks and pebbles. The latter were thus interpreted to be less coated. These authors also examined stratigraphic relations for these shape and size classes. Lobate, knobby, angular rocks and pebbles were observed to lie on top of other rocks and to exhibit less of a 600 nm inflection, a lower red/blue ratio, and a lower 530 nm band depth than other rocks. All of this spectral evidence is consistent with these classes of rocks being the least coated among those studied at the MPF site. Murchie *et al.*(2001) concluded that tabular and angular rocks were emplaced first and developed coatings; lobate and knobby rocks were emplaced later, perhaps when the environment was not as conducive (drier, colder) to the formation of cementing mineral rock coatings. This model is consistent with the multi-stage model for coating and soil formation suggested by McSween *et al.*(1999).

A related model was developed by Bishop *et al.*(2002) using a combination of IMP spectral data, APXS chemical results, results from the MPF magnet experiment (Madsen *et al.*, 1999), and laboratory studies of martian analog materials to study the nature of the bright drifts, possibly cemented or indurated soils, and rock coatings observed at the MPF landing site. They suggested that mobile dust particles can account for the spectral and chemical properties of bright drifts observed at the MPF landing site and that this same dust, containing reactive sulfate and/or ferric oxyhydroxide phases, has also coated the rocks. Bishop *et al.*(2002) postulated that indurated soils and cemented coatings on rocks have formed in locations where these reactive components have interacted with soil or rock surfaces for the longest amount of time. In their model, iron

oxyhydroxide minerals and sulfate salts, carried in the mobile dust, coat bare rock surfaces and form bonds (several types of bonds are possible: OH-cation, O-Si or O-cation) with the rock surface to form an indurated coating. Chemical reaction or cementing of the dust/soil particles to the rock surfaces would also darken the spectra compared to rocks simply coated by a layer of dust/soil particles based on the results of lab experiments of cemented fines (Bishop *et al.*2002). The laboratory samples prepared by Bishop *et al.*(2002) utilized mixtures of synthetic iron oxyhydroxide-montmorillonite soils, natural sulfate-bearing volcanic soils and hydrated magnesium sulfate in varying proportions. These mixtures had magnetic susceptibilities on the order of what was observed for the dust at the MPF site.

The spectral character of Maroon Rock resembles that of IMP soils and is believed to be a coating composed of soil-like materials. Like Brown Soil, the Maroon Rock spectral glass is a "secondary trend" material (McSween *et al.*, 1999) and could contain the same distinguishing mineralogic components discussed previously with regards to the nature of the secondary trend materials. The lower albedo of Maroon Rock spectra relative to that of Brown Soil could also be significant. As noted above, a chemically-bound coating of volcanic fines would be expected to have a darker spectrum than that of the loose fines (Bishop *et al.*, 2002). Thus, the Maroon Rock spectrum is consistent with an optically thick coating of fines that has reacted with the rock surface to form a hardened coating akin to a desert varnish.

12.3.5 IMP photometric observations

As described in a companion chapter (Johnson *et al.*, 2006), the IMP was used during the MPF mission to acquire VNIR images of rocks and soils over a wide range of illumination geometries. Johnson *et al.*(1999) modeled these data using a Hapke radiative transfer model (Domingue *et al.*, 1997) to study the photometric and physical properties of materials at the landing site over phase angles from ~0° to ~155°. Johnson *et al.*(1999) concluded that the photometric functions of the soils and dust-coated rocks were dominantly backscattering, with single scattering albedos similar to those observed at the Viking Lander sites (e.g., Arvidson *et al.*, 1989; Guinness *et al.*, 1997). Mixture modeling using single scattering albedos suggested that lighter-toned "Red" rock surfaces were a combination of dust, soil, and lower albedo "Gray" rock types. This was consistent with the hypothesis noted previously that the Red Rock class represented Gray Rocks coated with dust and soil materials. The Gray Rocks also exhibited more forward scattering signatures suggestive of surfaces more consistent with laboratory measurements of rough, clear spheres with few internal scatterers (McGuire and Hapke, 1995). This was consistent with qualitative comparisons of phase curves for the Gray Rocks, which indicated surfaces that were smooth on the centimeter to millimeter scale. The hypothesis advanced by Johnson *et al.*(1999) was that the surfaces of Gray Rocks were covered by a smooth coating similar to terrestrial varnished rock surfaces and/or a glassy rind. Bridges *et al.*(2001) noted that the forward scattering behavior of these rocks could also be consistent with an eolian polish on these rock surfaces. Ratios of reflectance spectra of the same rock surfaces acquired under different lighting conditions by Johnson *et al.*(1999) suggested that the major difference between spectra acquired at different times of day was in their overall reflectance values. However, subtle spectral differences at wavelengths <600 nm were thought to be the result of either residual

atmospheric lighting effects or wavelength-dependent variations in the modeled photometric functions.

12.3.6 Classification of the IMP SuperPan

In order to obtain more comprehensive statistics on spectral classes contained in the IMP Super Pan and to search for potential new classes and obtain new perspectives on the distribution of known spectral classes, a number of octants in the SuperPan have been analyzed with a self organizing map artificial neural network (ANN) classification approach (Farrand *et al.*, 2004; 2005; Merényi *et al.*, 2004). The ANN processing architecture used is a hybrid network. ANN architectures consist of simple processing elements or neurons, structured into an input layer, an output layer, and one or more hidden layers, with each layer partially or fully connected to the next. The hidden layer in the architecture used by these workers was a two-dimensional Self-Organizing Map (SOM), modified from that originally developed by Kohonen (1988). The SOM hidden layer, whose function is clustering, was coupled with a categorization learning output layer, which was used to perform supervised classification. This approach for classification differs from previous studies which categorized the data set in terms of spectral parameters (e.g., McSween *et al.*, 1999; Bell *et al.*, 2000) and those that had examined the spectral variability of the data through SMA (Bell *et al.*, 2002). Examination of spectral parameters was useful for relating the spectral properties of materials in the scene to known terrestrial analogs (e.g., Morris *et al.*, 2000) and determining spectral trends in the data (McSween *et al.*, 1999). Analysis through SMA was useful in determining the major and minor materials that contributed to the spectral variability of the data set and for determining small scale anomalous materials in the scene (such as the isolated occurences of Black Rock). Application of the SOM ANN approach was used to actually produce class maps of the data where spectrally unique and mappable classes were determined and pixels in the Super Pan were assigned to these classes. This effort differs from previous studies in that, for example, examination of spectral parameter trends do not map out specific classes and the SMA fraction images map out only a small number of endmember classes. A larger number of classes with subtle spectral differences are mapped out in the SOM ANN classification. As noted earlier, such class maps can be used to gather improved statistics on major spectral surface units and to observe spatial trends in these classes.

Analysis of the S0184 octant (right eye class map shown in Figure 12.11) revealed several interesting trends, including the need for incorporating two Black Rock classes to the models, each with distinct spectra. Several classes covered occurrences of Gray Rock as well; however, as noted above, there are several morphologic classes, each with the spectral designation of "Gray Rock". Several distinct soil classes were distinguished through the user directed clustering approach. These included the broadly distributed bright red drift soils, the darker "rock soil" (Bell *et al.*, 2002), and other dark soils. Intriguingly, the classification hints at layering in the distant Twin Peaks. Figure 12.12b shows the left eye classification map that zooms in on South Twin Peak. There are three classes that are most abundant in the far field. Class M (purple) is associated with the top of North and South Twin Peak and classes b (aquamarine) and K (cyan) cover much of the rest of the far field. Averages of these classes from the S0183 left scene indicate that class M has a shallow 900 nm absorption. Classes b and K are similar with b having a flatter NIR spectrum than K. In the near field, classes b and K can be

associated with the "rock soil" class noted above and by Bell *et al.*(2002). The class M spectra, associated with the upper portion of the Twin Peaks shares common spectral features with that of near field examples of Brown Soil (Figure 12.13) with both having a pronounced kink at 530 nm and a broad long wavelength absorption centered at 930 nm. As was noted above, Brown Soil is a material on the "secondary" spectral trend along with Maroon Rocks and these secondary trend materials have been suggested to contain a ferric oxide phase absent from the "primary" trend materials such as a ferrihydrite, maghemite, or hematite/pyroxene mixtures (McSween *et al.*, 1999) or goethite (Barnouin-Jha *et al.*, 2000; Murchie *et al.*, 2001). Thus, this distinguishing component from the secondary trend materials might also be a prominent constiuent of the upper tiers of the Twin Peaks.

12.4 Summary

The view that has emerged from analysis of the data provided by the MPF IMP and other MPF experiments is one of a field site generally similar to pre-landing expectations, but in detail consisting of unexpected features. Perhaps most important among the surprises was that the expectation that a "grab-bag" of rock types would be present was largely unfulfilled. All rocks examined by the APXS on-board the Sojourner rover had similar chemical compositions, interpreted to be volcanic basalts or basaltic andesites (see Chapter 3 by Foley *et al.*). The IMP data were important in relating the spectral characteristics of the small number of rocks examined by the APXS to the vastly larger number of rocks observed at the site. Initial analysis of the IMP data indicated that all of the "cleanest" or minimally coated rock surfaces could be classified into a single "Gray Rock" spectral class. Gray Rocks all appear to have varying degrees of "contamination" by ferric oxide and sulfur-bearing dust coverings and/or coatings. Photometric models have suggested that the Gray Rock surfaces may have glassy rinds or eolian polished surfaces (Johnson *et al.*, 1999; Bridges *et al.*, 2000). However, post-mission analysis of IMP Super Pan data (Murchie *et al.*, 2000; Bell *et al.*, 2002) revealed a small population of small rocks and rocky fragments/clasts (the "Black Rock" spectral class) that differ from the Gray Rock spectral class in that they exhibit a shorter wavelength relative reflectance maximum and a shorter wavelength NIR absorption band than the prevailing Gray Rock spectral class. These rare Black Rock materials may be endmembers that represent the least altered, least coated samples of "pristine" rock at the MPF site or could represent a distinct lithology transported to the field site by the catastrophic Ares Vallis flood. Unfortunately, the unique spectral character of these rocks was not recognized until after the mission had ended and were never examined *in situ* by the APXS.

Soils at the landing site were originally classified in detail by Bell *et al.*(2000), but can be more generally grouped into 4 broad classes: Bright Red Drift, Brown Soil, Dark Soil, and Disturbed Soil. Analysis of the Bright Red Drift material by the APXS showed that it was chemically similar to the reddish drifts measured at the Viking landing sites (*e.g.,* Clark *et al.*, 1982), and it has since been shown to be chemically similar to the reddish drifts examined by the MER rovers (*e.g.,* Rieder *et al.*, 2004). IMP data indicated that this material lacked a well defined absorption in the 900 nm region. However, Brown Soil, which was often associated with putatively indurated or more cohesive soil deposits (Bell *et al.*, 2002) was observed to have a weak 900 to 930 nm absorption band.

Some Dark Soil exposures, such as that seen on the eolian "Mermaid" duneform, were also observed to have a weak band with a 930 nm band minimum. The similarity between Dark Soil spectra and that of telescopic martian dark region spectra such as Oxia Palus (*e.g.,* Mustard and Bell, 1994) led Morris *et al.*(2000) to suggest that these Dark Soils might be spectrally dominated by low-Ca pyroxenes (orthopyroxene and/or pigeonite). By analogy with observation of similar bedforms studied by the Spirit rover, these could be surfaces armored by low-Ca pyroxene rich pebbles (*e.g.,* Bell *et al.*, 2004; Farrand *et al.*, 2005). While the overall MPF landing site has been categorized as one that is of intermediate albedo and with characteristics intermediate between the TES surface type 1 and surface type 2 areas (Wyatt *et al.*, 2003), the armored dune surfaces have spectral properties similar to larger dark regions to the south and thus provide some insight into what the nature of those larger dark regions might resemble. By analogy, larger dark regions could consist of broader expanses of coarse grained basaltic clasts that form armored dunes such as Mermaid. The Meridiani Planum dark region examined by the Mars Exploration Rover Opportunity has likewise found a region with coarse grained sands and armored duneforms (Squyres *et al.*, 2004; Soderblom *et al.*, 2004).

The MPF IMP results provide a view of a portion of the martian surface directly affected by the catastrophic outflows that were important in shaping large expanses of Mars' northern hemisphere. The different types of rock coatings observed by the IMP can be explained in terms of there being environmentally distinct periods in Mars' past. The separation between the "primary" and "secondary" trend materials is indicative of different mineral constituents in each. This evidence, in combination with the observations that different shape classes of rocks have different spectral properties and that rocks with less of a 600 nm inflection are stratigraphically higher than those with more of a 600 nm inflection indicate that lobate and knobby rocks may have been emplaced later than tabular, angular and equant rocks and that the lack of a 600 nm inflection is consistent with a colder, drier climate less conducive to the formation of cementing mineral rock coatings. The presence of materials similar to the secondary trend materials on the upper tiers of the Twin Peaks might also indicate that the peaks represent older material. It can also be inferred that rocks that appear to have minimal to no coatings, primarily the Black Rock spectral class, have likely been in that type of state for some time. The persistence of such dry, dessicating conditions is consistent with observations by the Mars Exploration Rovers Spirit and Opportunity of abundant olivine and magnetite in the soils at both landing sites (Yen *et al.*, 2005; Morris *et al.*, 2004; 2006) and observations of crater degradation at the Spirit site that indicate low erosional rates (Golombek *et al.*, 2006).

References:

Adams, J. B., Smith, M. O., and Gillespie, A. R. (1993). Imaging spectroscopy: Interpretation based on spectral mixture analysis. In *Remote Geochemical Analysis: Elemental and Mineralogical Composition*, ed. C. M. Pieters and P. A. J. Englert, New York: Cambridge University Press, p. 145-146.

Adams, J. B., Smith, M. O. and Johnson, P. E. (1986). Spectral mixture modeling: A new analysis of rock and soil types at the Viking Lander 1 site. *J. Geophys. Res.*, **91**, B8, p. 8098-8112.

Allen, C. C., Morris, R. V., Jager, K. M., *et al.*(1998). Martian regolith simulant JSC Mars-1. *Lunar Plan. Sci. Conf. XXIX*, #1690.

Arvidson, R. E., Guinness, E. A., Dale-Bannister, M. A., Adams, J. B., Smith, M. O., Christensen, P. R., and Singer, R.B. (1989). Nature and distribution of surficial deposits in Chryse Planitia and vicinity, Mars. *J. Geophys. Res.*, **94**, 1573-1587.

Bandfield, J. L., Hamilton, V. E. and Christensen, P. R. (2000). A global view of Martian surface compositions from MGS-TES. *Science*, **287**, 1626-1630.

Barnouin-Jha, O., Murchie, S., Johnson, J. R., Bell, J. F. III, and Morris, R. V. (2000). Rock coatings at the Mars Pathfinder landing site. *Lunar and Planetary Science XXXI*, Abstract #1267.

Bell III, J. F., Farrand, W. H., Johnson, J. R. and Morris, R. V. (2002). Low abundance materials at the Mars Pathfinder landing site: An investigation using spectral mixture analysis and related techniques. *Icarus*, **158**, 56-71.

Bell III, J. F., McSween, H. Y. Jr., Murchie, S. L., *et al.* (2000). Mineralogic and compositional properties of Martian soil and dust: Results from Mars Pathfinder. *J. Geophys. Res.*, **105**, 1721-1755.

Bell III, J. F*.,* Squyres, S. W., Arvidson, R. E., *et al.* (2004). Pancam multispectral imaging results from the Spirit rover at Gusev crater. *Science,* **305***,* 800-806.

Bishop, J. L., Schiffman, P., Dyar, M. D., Lane, M. D., Murad, E. and Drief, A. (2006). Soil forming processes on Mars as determined by mineralogy: Analysis of recent Martian spectral, chemical, and magnetic data and comparison with altered tephra from Haleakala, Maui. *Lunar and Planetary Science XXXVII*, Abstract #1423.

Bishop, J. L., Parente, M. and Hamilton, V. E. (2003a). Identifying minerals on Mars through VNIR and Mid-IR spectral deconvolution based on the Martian meteorites. *Eos Trans. AGU,* **84**(46), Fall Mtg. Suppl., Abstract P21B-0045.

Bishop, J. L., Minitti, M. E., Lane, M. D. and Weitz, C. M. (2003b). The influence of glassy coatings on volcanic rocks from Mauna Iki, Hawaii and applications to rocks on Mars. *Lunar and Planetary Science XXXIV*, Abstract #1516.

Bishop, J. L., Murchie, S. L., Pieters, C. M. and Zent, A. P. (2002). A model for formation of dust, soil, and rock coatings on Mars: Physical and chemical processes on the Martian surface. *J. Geophys. Res.*, **107**(E11), 5097, doi:10.1029/2001JE001581.

Bishop, J. L. and Murad, E. (1996). *Mineral Spectroscopy: A Tribute to Roger G. Burns* (Special Publication, No. 5), eds. M. D. Dyar, C. McCammon, and M. W. Schaefer, The Geochemical Society, Houston, TX, p. 337-358.

Calvin, W. and Bell, J.F. III (2006). Mars surface composition: Historical context. In *The Martian Surface: Composition, Mineralogy, and Physical Properties,* ed. J.F. Bell III, Cambridge University Press, in press.

Clark, B. C., Baird, A. K., Weldon, R. J., Tsusaki, D. M., Schnabel, L. and Candelaria, M. P. (1982). Chemical composition of Martian fines. *J. Geophys. Res.*, **87***,* 10,059-10,067.

Deal, K. S., Arvidson, R. E. and Jolliff, B. L. (2003). Remote mapping of the Ja'u Desert, Hawaii: Silica in a Mars analog terrain. *Lunar Planet. Sci. XXXIV*, Abstract #1952.

Farrand, W. H., Bell, J. F. III, Johnson, J.,R., Squyres, S. W., Soderblom, J., Ming, D. W. (2006). Spectral variability among rocks in visible and near infrared multispectral Pancam data collected at Gusev Crater: Examinations using spectral mixture analysis

and related techniques. *J. Geophys. Res. - Planets*, **111**, E02S15, 10.1029/2005JE002495.

Farrand, W. H, Merényi, E., Murchie, S., Barnouin-Jha, O. S. (2005). Spectral class distinctions observed in the MPF IMP SuperPan using a self-organizing map. *Lunar and Planetary Science XXXVI*, Abstract #2009.

Farrand, W. H., Merényi, E., Murchie, S., Barnouin-Jha, O., and Johnson, J. (2004). Mapping rock and soil units in the MPF Superpan using a Kohonen self-organizing map. *Lunar and Planetary Science XXXV*, Abstract #1916.

Farrand, W. H., Johnson, J. R., Bell, J. F. III (2001). N-Dimensional visualization and spectral mixture analysis applied to Imager for Mars Pathfinder data: Detection and mapping of rocks and soils. *Lunar and Planetary Science XXXII*, Abstract #1656.

Farrand, W. H. and J. C. Harsanyi (1997). Mapping the distribution of mine tailings in the Coeur d'Alene River Valley, Idaho through the use of a Constrained Energy Minimization technique. *Rem. Sens. of Env.* **59**, p. 64-76.

Foley, C. N., Economou, T. E., Clayton, R. N. (2003). Final chemical results from the Mars Pathfinder alpha proton X-ray spectrometer**,** *J. Geophys. Res.,* **108**, E12, 10.1029/2002JE002019.

Foley, C. N., Economou, T. E., Clayton, R. N., Brückner, J., Dreibus, G., Rieder, R., and Wänke, H. (2006). Martian surface chemistry: APXS results from the Pathfinder landing site. In *The Martian Surface: Composition, Mineralogy, and Physical Properties,* ed. J.F. Bell III, Cambridge University Press, in press.

Gaddis, L., Kirk, R., Johnson, J., *et al.* (1999). Digital mapping of the Mars Pathfinder landing site: Design, acquisition, and derivation of cartographic products for science applications. *J. Geophys. Res*., **104**, 8853-8868.

Golombek, M. P., Cook, R. A., Moore, H. J., Parker, T. J. (1997a). Selection of the Mars Pathfinder landing site. *J. Geophys. Res.*, **102**, 3967-3988.

Golombek, M. P., Cook, R. A., Economou, T., *et al.* (1997b). Overview of the Mars Pathfinder mission and assessment of landing site predictions. *Science,* **278**, 1743-1748.

Golombek, M. P., Moore, H. J., Haldemann, A. F. C., Parker, T. J. and Schofield, J. T. (1999). Assessment of Mars Pathfinder landing site predictions. *J. Geophys. Res*., **104**, 8585-8594.

Golombek, M. P., Crumpler, L. S., Grant, J. A., *et al.* (2006). Geology of the Gusev cratered plains from the Spirit rover transverse. *J. Geophys. Res.*, **111**, E02S07, 10.1029/2005JE002503.

Guinness, E. A., Arvidson, R. E. and Clark, I. H. D. and Shepard, M. K. (1997). Optical scattering properites of terrestrial varnished basalts compared with rocks and soils at the Viking Lander sites. *J. Geophys. Res.*, **102**, 28687-28703.

Hamilton, V. E., Christensen, P. R. and Bandfield, J. L. (2003). Volcanism or aqueous alteration on Mars? (Communication Arising), *Nature,* **421**, 711-712; doi:10.1038/421711b.

Hapke, B. (1993). *Theory of Reflectance and Emittance Spectroscopy*, Cambridge University Press, 455 p.

Herkenhoff, K. E., Johnson, J. R. and Weller, L. A. (2003). The Imager for Mars Pathfinder Insurance Pan. In *The Sixth International Conference on Mars*, Abstract #3224.

Huck, F. O., Jobson, D. J., Park, S. K., *et al.* (1977). Spectrophotometric and color estimates of the Viking lander sites. *J. Geophys. Res.*, **82**, 4401-4411.

Johnson, J. R., Kirk, R., Soderblom, L. A., *et al.* (1999). Preliminary results on photometric properties of materials at the Sagan Memorial Station, Mars. *J. Geophys. Res.,* **104**, 8809-8830.

Johnson, J. R. and Grundy, W. M. (2001). Visible/near-infrared spectra and two-layer modeling of palagonite-coated basalts. *Geophys. Res. Lett.*, **28**, 2101-2104.

Johnson, J. R., Grundy, W. M. and Lemmon, M. T. (2003). Dust deposition at the Mars Pathfinder landing site: Observations and modeling of visible/near-infrared spectra. *Icarus*, **163**, 330-346.

Johnson, J. R., Bell, J. F. III, Geissler, P., *et al.* (2006). Physical properties of the martian surface from spectrophotometric observations. Ch. 19, *in The Martian Surface: Composition, Mineralogy, and Physical Properties*, Cambridge University Press.

Klaasen, K. P., Thorpe, T. E., and Morabito, L. A. (1977). Inflight performance of the Viking visual imaging subsystem. *Appl. Optics*, **16**, 3158-3170.

Kraft, D., Sharp, T. G. and Michalski, J. R. (2003). Thermal emission spectra of silica-coated basalt and considerations for Martian surface morphology. In *Lunar Planet. Sci. XXXIV*, #1420.

McGuire, A. F., and Hapke, B. W. (1995). An experimental study of light scattering by large, irregular particles. *Icarus*, **113**, 134-155.

McSween, H. Y. Jr., Murchie, S. L., Crisp, J. A., *et al.* (1999). Chemical, multispectral, and textural constraints on the composition and origin of rocks at the Mars Pathfinder landing site, *J. Geophys. Res.,* **104***, 8679-8716.

Merényi, E., Jain, A., Farrand, W. H. (2004). Applications of SOM magnification to data mining. *WSEAS Trans. on Systems*, **3**(5), 2122-2128.

Minnitti, M., Mustard, J. and Rutherford, M. (2002). Effects of glass content and oxidation on the spectra of SNC-like basalts: Applications to Mars remote sensing. *J. Geophys. Res.*, **107**, 10.1029/2001JE001518.

Morris, R. V., Klingelhöfer, G., Bernhardt, B., *et al.* (2004). Mössbauer mineralogy on Mars: First results from the *Spirit* landing site in Gusev Crater. *Science*, **305**, 833-836.

Morris, R. V., Golden, D. C., Bell, J. F. III, *et al.* (2000). Possible products of hydrolytic, hydrochloric, and sulfuric weathering at the Mars Pathfinder landing site: Evidence from multispectral, elemental, and magnetic data on analogue and meteorite samples. *J. Geophys. Res.,* **105***, 1757-1817.

Morris, R. V., Golden, D. C., Bell, J. F. III, and Lauer, H. V. (1995). Hematite, pyroxene, and phyllosilicates on Mars: Implications from oxidized impact melt rocks from Manicouagan Crater, Quebec, Canada. *J. Geophys. Res.*, **100**, 5319-5328.

Morris, R. V. and Neely, S. C. (1982). Optical properties of hematite-magnetite mixtures: Implications for Mars. *Lunar Planet. Sci. XIII*, 548-549.

Moore, H.J ., Bickler, D. B., Crisp, J. A., *et al.*(1999). Soil-like deposits observed by Sojourner, the Pathfinder rover. *J. Geophys. Res.,* **104**, E4, 8729-8746.

Murchie, S., Barnouin-Jha, O., Barnouin-Jha, K., *et al.* (2003). New insights into the geology of the Mars Pathfinder landing site from spectral and morphologic analysis of the 12-color Superpan panorama. In *The Sixth International Conference on Mars*, Abstract #3060.

Murchie, S., Barnouin-Jha, O., Johnson, J. R., Bell, J. F. III, McSween, H. Y. Jr., and Morris, R.V. (2000). Diverse rock types at the Mars Pathfinder landing site. *Lunar Planet. Sci. XXXI*, #1267.

Murchie, S., Barnouin-Jha, O., Johnson, J., Bell, J. F. III, and Morris, R.V. (2001). Spectral differences between shape classes of rocks at the Mars Pathfinder landing site. In *Lunar and Planet. Sci. XXXII,* Abstract #1825.

Mustard, J. F., Poulet, F., Gendrin, A., *et al.* (2005). Olivine and pyroxene diversity in the crust of Mars. *Science*, **307**, 1594-1597.

Mustard, J. F., Murchie, S., Erard, S. and Sunshine, J. (1997). In situ compositions of Martian volcanics: Implications for the mantle. *J. Geophys. Res.,* **102***,* 25,605-25,615.

Mustard, J. F. and Bell, J. F. III (1994). New composite reflectance spectra of Mars from 0.4 to 3.14 µm. *Geophys. Res. Lett.,* **21***,* 353-356.

Rieder, R., Economou, T., Wanke, H., *et al.* (1997). The chemical composition of martian soil and rocks returned by the mobile alpha proton X-ray spectrometer: Preliminary results from the X-ray mode. *Science*, **278**, 1771-1774.

Rieder, R., Gellert, R., Anderson, R. C., *et al.* (2004). Chemistry of Rocks and Soils at Meridiani Planum from the Alpha Particle X-ray Spectrometer. *Science,* **306***,* 1746-1749.

Roush, T. L., Blaney, D. L., and Singer, R. B. (1993). The surface composition of Mars as inferred from spectroscopic observations. In *Remote Geochemical Analysis: Elemental and Mineralogical Composition*, ed. C. M. Pieters and P. A. J. Englert, New York: Cambridge University Press, 367-393.

Singer, R. B. (1985). Spectroscopic observations of Mars. *Adv. Space Res*., **5**, 59-68.

Singer, R. B., McCord, T. B., Clark, R. N., Adams, J. B., and Huguenin, R. L. (1979). Mars surface composition from reflectance spectroscopy: A summary. *J. Geophys. Res*., **84**, 8415-8426.

Smith, P. H., Tomasko, M. G., Britt, D., *et al.* (1997a). The Imager for Mars Pathfinder experiment. *J. Geophys. Res.,* **102***,* 4003-4025.

Smith, P. H., Bell, J. F. III, Bridges, N. T., *et al.* (1997b). Results from the Mars Pathfinder camera. *Science*, **278**, 1758-1765.

Soderblom, L. A. *et al.* (2004). Soils of Eagle Crater and Meridiani Planum at the Opportunity Landing Site. *Science*, **306**, 1723-1726.

Squyres, S W. *et al.*(2004). The Opportunity Rover's Athena science investigation at Meridiani Planum, Mars. *Science*, **306**, p. 1698-1702.

Sullivan, R., Greeley, R., Kraft, M., *et al.* (2000). Results of the Imager for Mars Pathfinder windsock experiment. *J. Geophys. Res.*, **105**, 24547-24562.

Tanaka, K. L. (1997). Sedimentary history and mass flow structures of Chryse and Acidalia Planitiae, Mars. *J. Geophys. Res*., **102**, 4131-4150.

Thomas, N., Markiewicz, W. J., Sablotny, R .M., *et al.* (1999). The color of the Martian sky and its influence on the illumination of the Martian surface, *J. Geophys. Res.*, **104**, 8795-8808.

Wadhwa, M., Lentz, R. C. F., McSween, H. Y. Jr., and Crozaz, G. (2001). A petrologic and trace element study of Dar al Gani 476 and 489: Twin meteorites with affinities to basaltic and lherzolitic shergottites. *Meteoritics and Planet. Sci*., **36**, 195-208.

Ward, A., Gaddis, L., Kirk, R., *et al.* (1999). General geology and morphology of the Mars Pathfinder landing site. *J. Geophys. Res*., **104**, 8555-8572.

Wright, S. P., Farrand, W. H., Rogers, D., and Merényi, E. (2005). The nature of the Mars Pathfinder "Black Rock" lithology: Comparisions with SNC meteorites and OMEGA spectral images of Chryse Planitia. *Eos Trans*. *AGU*, 86(52), Fall Meet. Suppl., Abstract P21B-0145.

Wyatt, M. B., McSween, H.Y., Moersch, J. E. and Christensen, P. R. (2003). Analysis of surface compositions in the Oxia Palus region on Mars from Mars Global Surveyor Thermal Emission Spectrometer observations. *J. Geophys. Res*., **108**(E9), 5107, doi: 10.1029/2002JE001986.

Wyatt, M. B. and McSween, H. Y. Jr. (2002). Spectral evidence for weathered basalt as an alternative to andesite in the northern lowlands of Mars. *Nature*, **417**, 263-266.

Yen, A. S. *et al.*(2005). An integrated view of the chemistry and mineralogy of martian soils. *Nature*, **436**, doi:10.1038/nature03637.

Zipfel, J., Scherer, P. Spettel, B., Dreibus, G. and Schultz, L. (2000). Petrology and chemistry of the new shergottite Dar al Gani 476. *Meteoritics and Planet. Sci*., **35**, 95 - 106.

Figure Captions:

Figure 12.1. Example Gray Rock spectra averaged over tens of pixels from the rocks Shark (top) and rock in front of Moe (bottom). Error bars on this and subsequent spectral plots represent the standard deviation of the mean for the pixel spectra averaged.
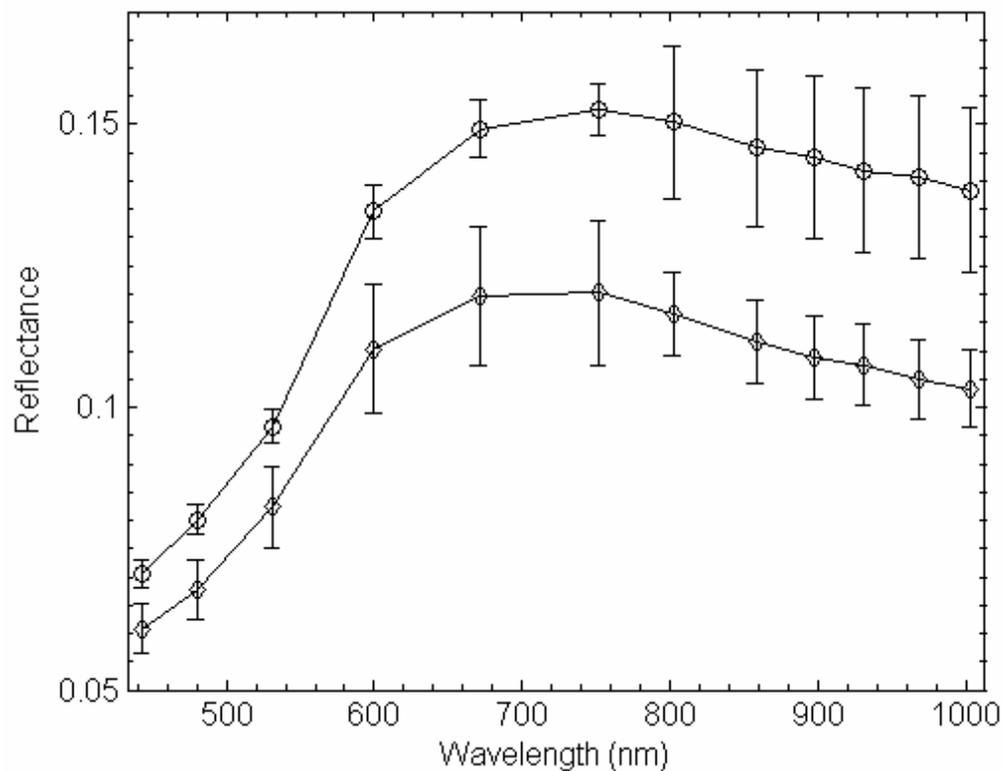
Figure 12.2. The IMP spectrum of the Gray Rock "Shark" compared against terrestrial analog materials which also display a negative NIR slope: a silica coating (Bishop *et al.*, 2003), a palagonitic tephra, HWHP301 (Morris *et al.*, 2000), and the clinopyroxene-rich SNC meteorite Nakhla (Morris *et al.*, 2000).
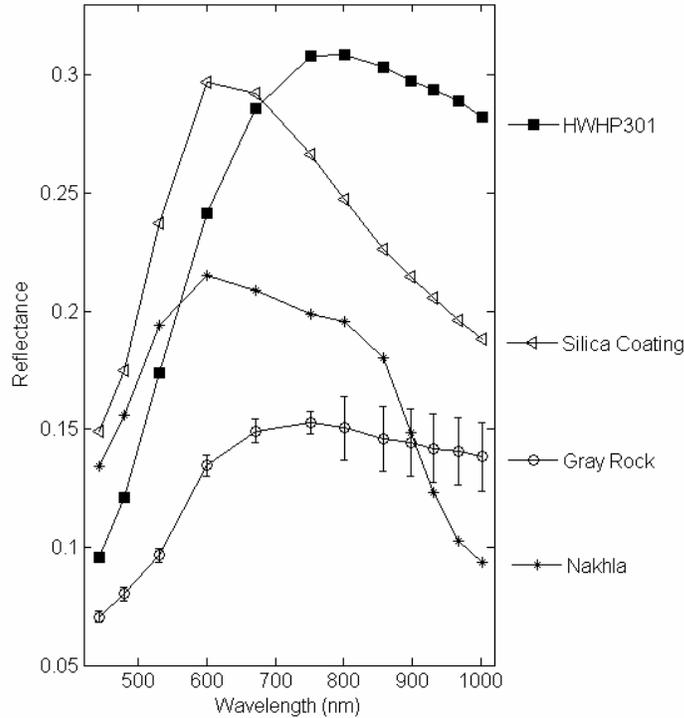
Figure 12.3. Orange and Black Rock spectra. Orange rock spectrum from SuperPan octant S0188 referenced by Murchie *et al.*(2000). Black rock spectrum from SuperPan octant S0184 (corresponds to Merenyi *et al.*(2004) class O).
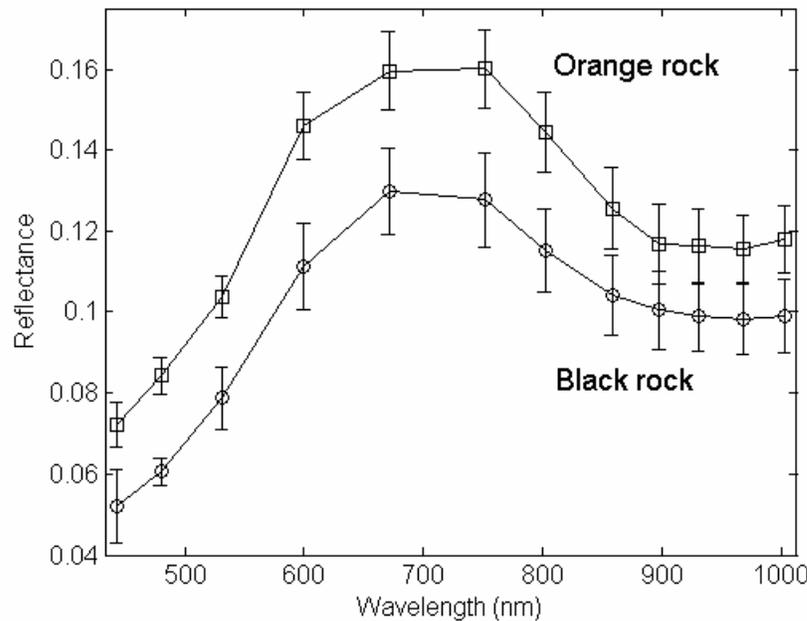
Figure 12.4. Fraction images and RMS error image from Spectral Mixture Analysis of a MPF component left eye image segment from the S0185 Super Pan octant. **A – C** represent, respectively the shade, bright drift, and rock image endmembers. **D** is the RMS error image. The bright rock with the high RMS error image is a detection of the Black Rock spectral class.
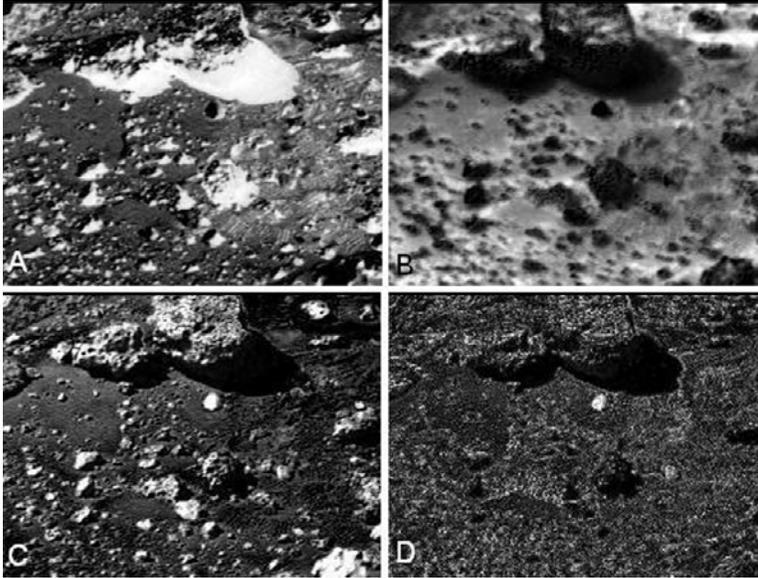
Figure 12.5. **A**. (top). 802, 671, and 443 nm composite of subset of octant S0183 centered on N. Twin Peak. **B**. (bottom) CEM fraction images highlighting occurences of Black Rock in far field of S0183 (see text).
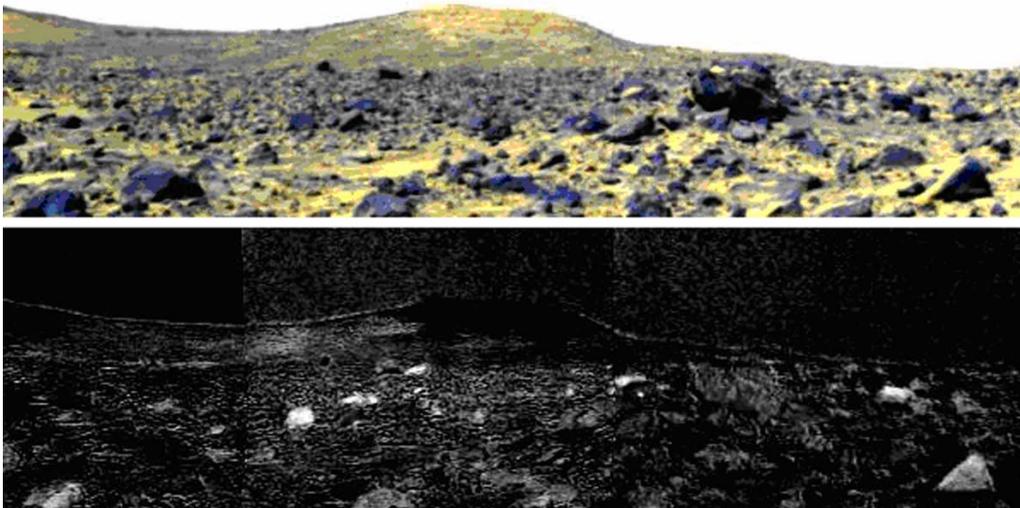
Figure 12.6. IMP Soil and Dust spectral units, from Bell *et al.*(2000).
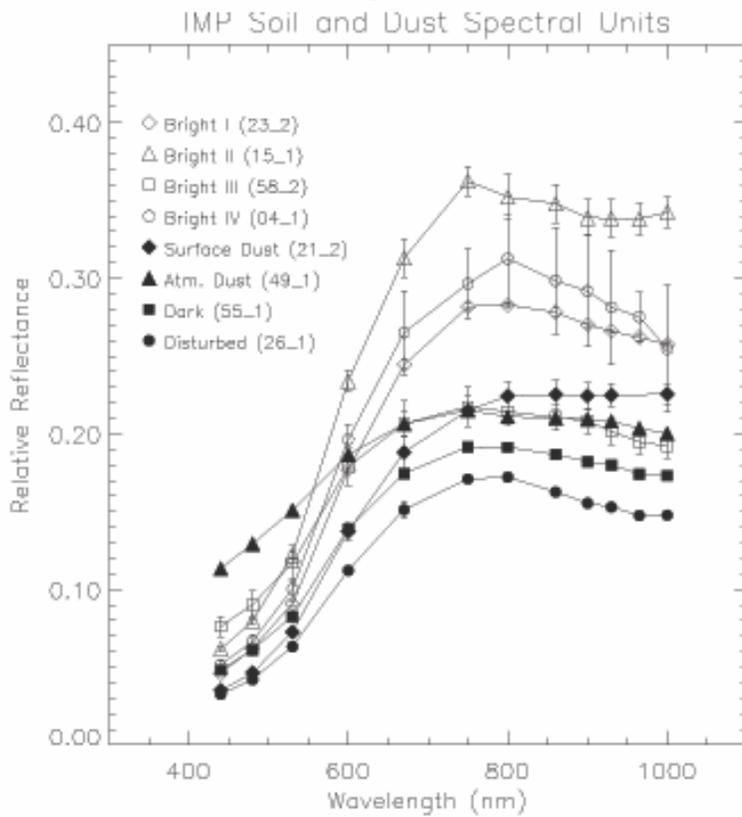
Figure 12.7. Comparison of Mermaid Dune spectrum to composite Oxia Palus spectrum, from Morris *et al.*(2000)
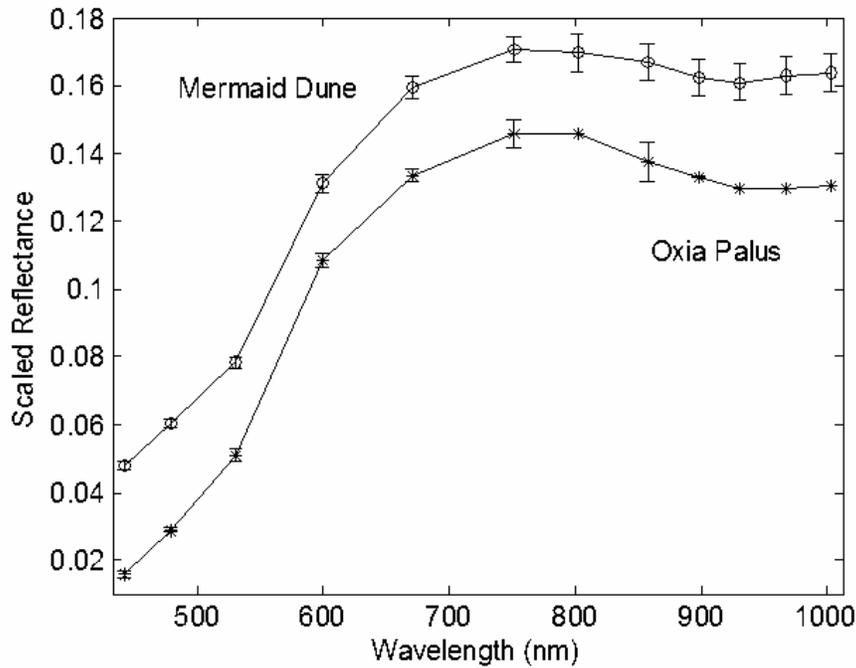
Figure 12.8. **A.** Bright Drift spectra extracted from the S0182 and S0185 Super Pan octants compared with a Haleakala loose fines spectrum (Hal-399) and the JSC-1 Mars simulant (Allen *et al.*, 1998). **B**. IMP Brown Soil spectrum from the S0186 Super Pan octant compared with terrestrial material that have a similar 930 nm band: a Mauna Kea jarositic tephra (the less than 5 µm fraction of HWMK 515; Morris *et al.*, 2000), a maghemite (MHS-3; Morris *et al.*, 2000), and a ferrihydrite (Ferrih. 46; Bishop *et al.*, 1998).
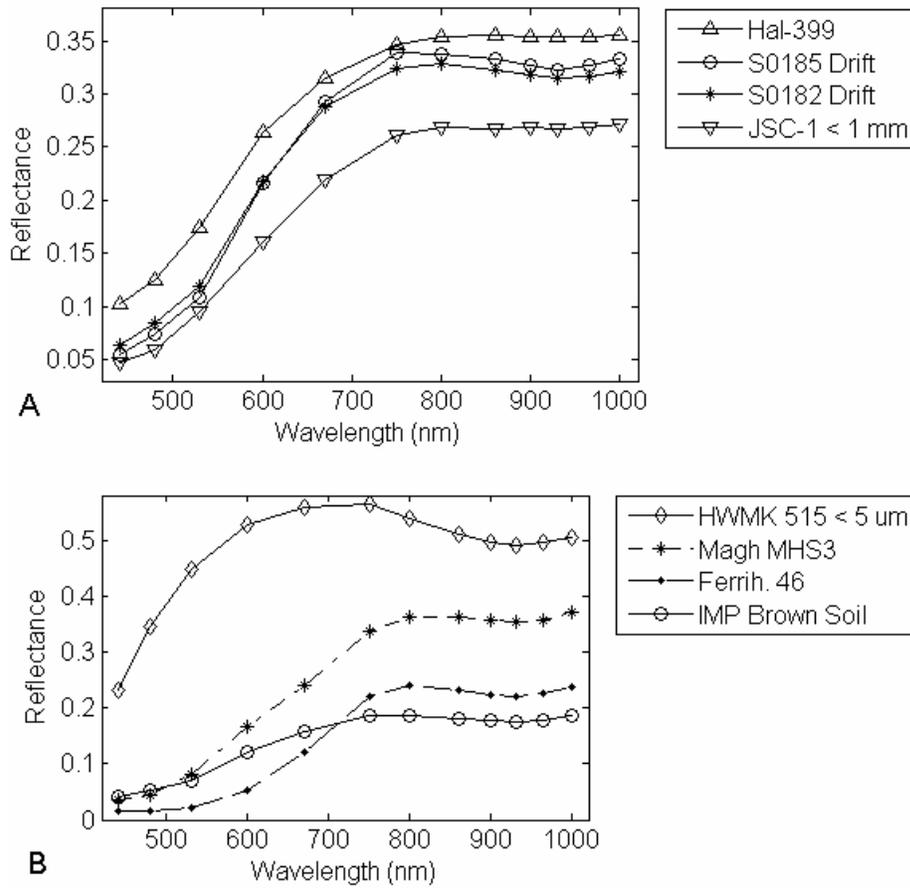
Figure 12.9. IMP spectra of Pink (Scooby Doo), Red (unnamed), Maroon, and Gray (Shark) rock spectra. For purposes of clarity, Pink rock has been offset upwards by 0.05; Red rock has been offset upwards by 0.02; Gray rock has been offset downwards by 0.05.
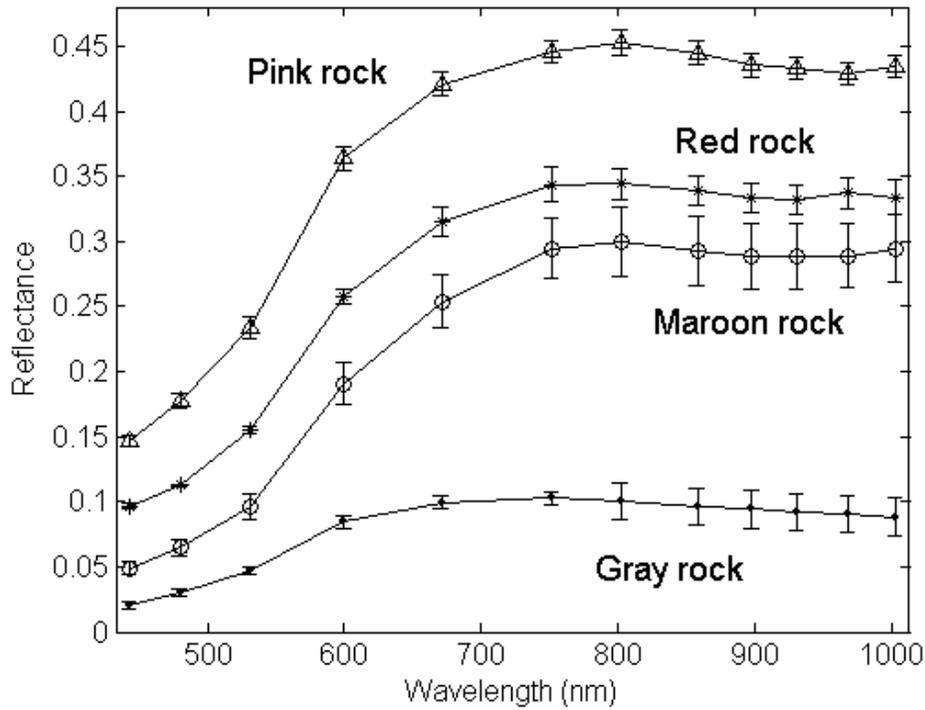

Figure 12.10. Spectral parameters used in the classification of Gray, Red, Maroon, and Pink rock types. Figure from McSween *et al.*(1999).
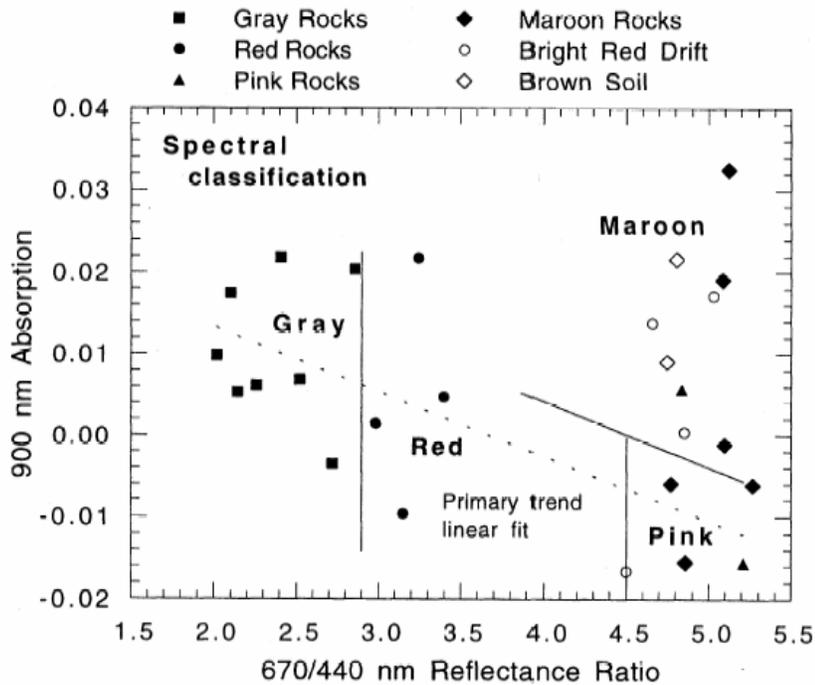
Figure 12.11. Classification map of the right eye data from the S0184 octant of the Super Pan. Classification was obtained through application of the self-clustering approach of the self organizing map ANN approach described by Farrand *et al.*(2005) and Merényi *et al.*(2004). Color bar represents key to classes.
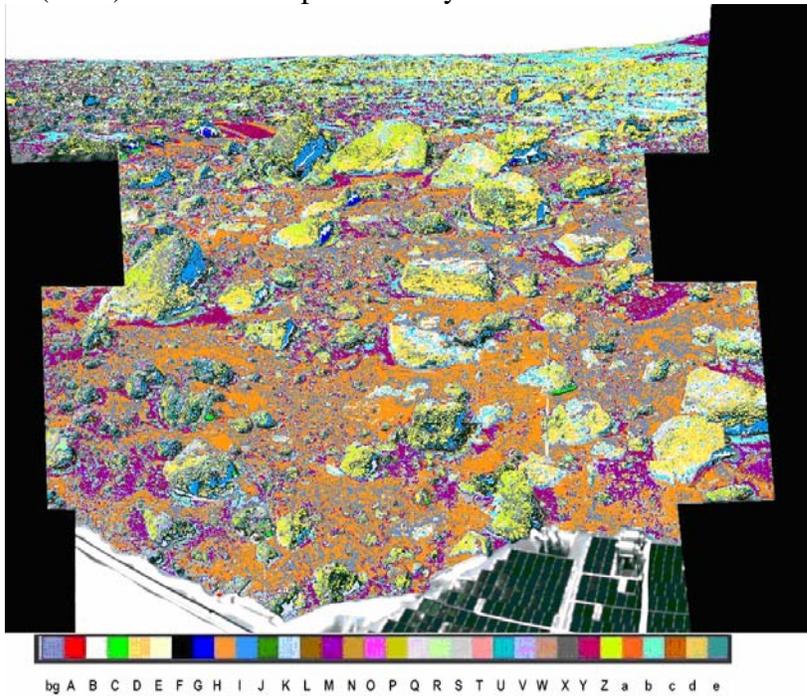

Figure 12.12. Top: Composite of left eye bands 802, 671, and 443 nm for far field portion of octant S0183. Bottom: Class map for the far field of S0183 (left eye data). Note the purple color (class M) associated with the top of North Twin Peak and prevalence of cyan colors of classes b and K in the far field.


451
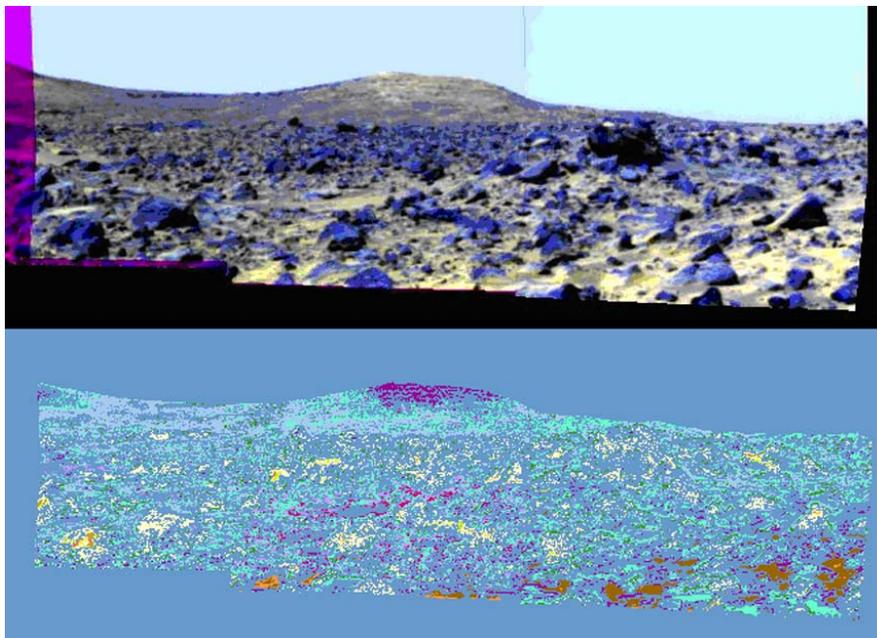
Figure 12.13. Comparison of the SOM/ANN class M spectrum averaged over the upper tiers of the Twin Peaks, compared to a near-field observation from the S0187 octant. Note similarity of the spectra in the 900 to 930 nm region and at the 530 nm kink and low curvature in the 600 nm region. The class M spectrum was offset upwards by 0.05 for clarity.